The European Master in Advanced Structural Analysis and Design using Composite Materials is a join initiative of:

Universidade do Minho

Universitat de Girona

Università degli Studi di Napoli Federico II

INSA Institut National des Sciences Appliquées Toulouse

Université de Toulouse

High-Velocity Impact Testing of Composites

Syed Hasnain Ali Pir Zada

FRP++ Advanced structural analysis and design using composite materials

UMinho | 2025

Universidade do Minho
Escola de Engenharia

Syed Hasnain Ali Pir Zada

High-Velocity Impact Testing of Composites

FRP++
Advanced structural analysis and design using composite materials

Funded by the European Union

September 2025

Universidade do Minho
Escola de Engenharia

Syed Hasnain Ali Pir Zada

High-Velocity Impact Testing of Composites

FRP++
Advanced structural analysis and design using composite materials

Master Dissertation
European Master Advanced Structural Analysis and Design using Composite Materials

Work developed under the supervision of
Doctor Luís Correia
Doctor Filipe Ribeiro

Funded by the European Union

September 2025

ACKNOWLEDGEMENTS

I would like to express my deepest and sincerest gratitude to my thesis supervisors, Dr. Luis Correia and Dr. Filipe Ribeiro for their invaluable guidance, continued support, and constant encouragement throughout the course of this research. Their expertise and constructive feedback have been essential in shaping the direction and quality of this dissertation.

I am sincerely grateful to the Erasmus Mundus MSc. FRP++ Committee for their financial support and for awarding me the scholarship that made this work possible.

I would also like to thank TEKEVER for providing the specimens used in this research and ISQ for granting access to their laboratories and testing facilities during the experimental campaign.

I would like to thank Dr. Mario Aruda for his guidance in the numerical modelling and simulation.

On a personal note, I am profoundly grateful to my family for their constant encouragement, unconditional love and support throughout this journey, with special thanks to my father, whose unwavering belief in me has been an enduring source of strength.

DECLARATION

Name: Syed Hasnain Ali Pir Zada

Email: syedhasnainpirzada@gmail.com

Phone number: +351 931317398

Citizen Card Number: AE3913871

Title of the Dissertation: High-Velocity Impact Testing of Composites

Supervisors:

Doctor Luís Correia

Doctor Filipe Ribeiro

Year of Conclusion: 2025

Master Course in Advanced Structural Analysis and Design using Composite Materials

University of Minho, 29/08/2025

Signature:

Ensaio de impacto de alta velocidade de compósitos

RESUMO

As estruturas aeronáuticas são particularmente vulneráveis a impactos de alta velocidade, como colisões com aves ou granizo, que podem causar danos severos e comprometer a segurança do voo. Assim, o desenvolvimento e a avaliação de materiais capazes de resistir a tais eventos são fundamentais para a segurança aeroespacial.

Esta dissertação investiga o comportamento de painéis compósitos sanduíche de CFRP com núcleo de espuma PET sujeitos a impactos de alta velocidade. Os painéis foram fabricados pela TEKEVER, uma empresa nacional líder na conceção e fabrico de aeronaves não tripuladas. Esferas de aço foram projetadas com recurso a um canhão pneumático com velocidades entre 55,9 e 197,8 m/s. Paralelamente, recorreu-se à modelação por elementos finitos (MEF) com recurso ao ABAQUS/Explicit para simular os impactos, com especial atenção à absorção de energia.

Os painéis ensaiados demonstraram ter uma capacidade de absorção de energia reduzida e baixa resistência ao impacto, com perfuração completa, mesmo na menor velocidade testada. As simulações numéricas reproduziram de forma razoável o comportamento global, mas apresenraram limitações pela escassez de informação mecânica sobre a espuma e por instabilidades numéricas a altas velocidades.

Os resultados evidenciam a limitada adequação desta configuração de painéis em condições severas de impacto. Recomenda-se o aumento da espessura das faces, uso de núcleos alternativos ou arquiteturas híbridas — de modo a melhorar a absorção de energia e ampliar a aplicabilidade destes materiais.

PALAVRAS-CHAVE: Materiais compósitos; impacto de alta velocidade; MEF; painel sanduíche; aeroespacial; núcleo de espuma

High-Velocity Impact Testing of Composites

ABSTRACT

Aircraft structures are highly susceptible to high-velocity impacts from projectiles such as drones and hail strikes, which can cause severe structural damage and compromise flight safety. Developing and assessing materials capable of withstanding such events is therefore critical for advancing aerospace safety and performance.

This dissertation investigates the behaviour of CFRP–PET foam core composite sandwich panels under high-velocity impacts. The panels, manufactured by TEKEVER, a leading Portuguese company in the design and production of unmanned aerial vehicles, were tested by launching steel spheres with a pneumatic gas gun at velocities 55.9 to 197.8 m/s. Complementary finite element analyses (FEA) were performed using ABAQUS/Explicit to simulate the impact response, with emphasis on energy absorption.

The sandwich panels exhibited limited energy absorption and poor impact resistance, with complete perforation occurring even at the lowest impact velocity. Numerical simulations captured the overall impact trends but were limited by the scarcity of foam material data and by numerical instabilities at higher velocities.

These findings highlight the limited suitability of thin CFRP–PET sandwich configurations for aerospace applications under severe impact conditions. Future work should prioritize extensive experimental validation, refined numerical models, and optimized sandwich architectures—such as increased face-sheet thickness, alternative core configurations, or hybrid materials —to improve energy absorption and broaden their applicability.

KEYWORDS: Composite materials; high-velocity impact; FEM; sandwich panels; aerospace; foam core

TABLE OF CONTENTS

LIST OF FIGURES

LIST OF TABLES

LIST OF ABBREVIATIONS AND SYMBOLS

Abbreviations

BVID	Barely Visible Impact Damage
CEL	Coupled Eulerian–Lagrangian
CFRP	Carbon-Fibre Reinforced Polymer
CT	Computed Tomography
COV	Coefficient of Variation
DIC	Digital Image Correlation
FEA	Finite Element Analysis
FEM	Finite Element Modelling
FML	Fibre-Metal Laminate
ICAO	International Civil Aviation Organization
PET	Polyethylene Terephthalate
SPH	Smoothed-Particle Hydrodynamics
VUMAT	Vectorized User Material
VUSDFLD	Vectorized User Subroutine for Definition of Field Variables

Symbols

θ	Angle between the two high-speed cameras during experimentation
α	Horizontal deviation of the projectile from the centre of the two cameras

1. INTRODUCTION

1.1. Motivation

Aircraft structures are highly vulnerable to high-velocity impacts from external projectiles such as drones and hailstones. According to the International Civil Aviation Organization (ICAO), more than 270,000 wildlife strike incidents were reported between 2016 and 2021 [1]. Majority collisions occur on contact with windscreens or jet aircraft engines generating estimated annual damages exceeding USD 1.2 billion for commercial aviation[2]. Following bird strikes, the danger of man-piloted drones are a primary concern. Around 100 to 150 near-collision reports regarding drones are filed each month. Drones also lack any robust mitigation and prevention systems, unlike special radar prevention systems for birds employed in larger airports and exhibit unpredictable movements with irregular paths making detection challenging [3]. In parallel, hail impacts represent another critical hazard. A hailstorm at Kandahar in April 2013, for example, damaged 80 helicopters—affecting rotors, electronics, and windows—with losses surpassing USD 1 million [4]. Hail strikes can shatter windshields, dent fuselage surfaces, and disable critical sensors, further underscoring the urgent need for impact-resistant materials in aerospace applications.

Composite sandwich structures, particularly those based on carbon fibre reinforced polymers (CFRPs), are increasingly used in aerospace due to their high strength-to-weight ratios. However, their performance under high-velocity impact remains a limiting factor, as such events can cause complex damage mechanisms including delamination, fibre fracture, and core crushing. While fibre-metal laminates (FMLs) and hybrid systems have demonstrated improved performance, the impact behaviour of CFRP–foam sandwich panels remains insufficiently characterised. Addressing this research gap is crucial to advancing the safety and resilience of next-generation aerospace structures.

This thesis aims to contribute to this field by investigating the high-velocity impact response of CFRP–PET foam (PET: Polyethylene Terephthalate) sandwich panels manufactured by

TEKEVER. By combining controlled experimental testing with finite element modelling (FEM), the study seeks to provide new insights into energy absorption mechanisms, failure modes.

1.2. Objectives

Although CFRP sandwich structures are widely used in aerospace, most high-velocity impact research has concentrated on honeycomb-core panels and hybrid fibre–metal systems. Studies on foam-core sandwiches exist but remain comparatively limited, particularly regarding PET foam cores, whose low-cost and recyclable nature make them increasingly attractive for aerospace applications. As a result, there is a knowledge gap concerning their energy absorption and damage mechanisms. This thesis addresses this gap by pursuing the following objectives:

i. Experimental characterisation of impact response:
   Perform controlled high-velocity impact tests on CFRP–PET sandwich panels using a pneumatic gas cannon with steel sphere projectiles, covering velocities from 55.9 to 197.8 m/s. This provides baseline data on penetration behaviour, failure modes, and residual projectile velocities.

ii. Material property determination for modelling input:
   Characterise the constituent materials (CFRP face sheets and PET foam core) to provide realistic input data for finite element modelling. This ensures that the simulations are grounded in experimentally measured parameters rather than generic assumptions.

iii. Finite element modelling and simulation:
   Develop a finite element model in ABAQUS/Explicit to simulate the high-velocity impacts observed experimentally. Particular attention is given to evaluating:
   - stress wave propagation and energy absorption mechanisms,
   - the influence of increasing impact velocity on structural response.

iv. Comparative evaluation of experimental and numerical results:
   Compare experimental outcomes with simulation results to assess the predictive capability and limitations of the numerical model. The analysis focuses on residual

velocity, observed damage patterns, and failure progression across the tested velocity range.

1.3. Structure of the Thesis

This dissertation is structured into five chapters, each addressing a distinct stage of the research process.

The first chapter introduces the project by outlining its motivation, objectives, and how the thesis is organised.

Chapter 2 presents the state of the art, providing a detailed review of the literature on high-velocity impact in composite structures, with particular attention to experimental studies, failure mechanisms, and numerical modelling techniques.

Chapter 3 details the methodology, covering the experimental programme—including fabrication of the CFRP–PET foam sandwich panels, specimen preparation, and high-velocity impact testing using a pneumatic gas gun—as well as the finite element modelling and simulation work conducted in Abaqus/Explicit. This section explains the modelling strategy, underlying assumptions, and computational setup.

Chapter 4 presents and discusses the results, integrating post-impact observations, calculations of residual velocity, tomographic analyses, and comparisons with numerical predictions. The final chapter.

Chapter 5 concludes the dissertation by summarising the main findings, discussing the limitations of the study, and offering recommendations for future research.

2. STATE OF THE ART

2.1. Physics of the High-Velocity Impact

High-velocity impact has been a subject of extensive study due to its relevance in the aerospace and defence industries where materials are exposed to extreme loading conditions. Researchers have focused on understanding how different materials absorb, dissipate, and transmit energy during such events, as this knowledge is critical for designing safer and more resilient structures [5]. High-velocity events involve complex physical phenomena including shock wave propagation, stress wave interactions, and strain rate-dependent deformation, making the problem highly nonlinear and dynamic in nature [6]. Capturing this behaviour requires not only experimental efforts but also advanced computational modelling techniques that account for transient, high-energy events within fractions of a second [7].

As an object is subjected to a high-velocity impact, the event unfolds over extremely short time scales, typically in the order of microseconds or milliseconds. During this time, the kinetic energy of the projectile is rapidly transferred to the target specimen, leading to intense localised stresses, high strain rates, and often, material failure. Unlike static loading, high-velocity impacts can induce shock waves that propagate through the material, causing complex stress distributions and potentially triggering brittle fracture, spallation, or plastic deformation depending on the material type. The impact response is heavily dependent on the strain rate sensitivity and stress wave interactions [6].

In metallic materials, the response to high-velocity impact tends to involve significant plastic deformation followed by possible adiabatic shear banding or even melting at the point of contact. Ductile metals may absorb considerable energy before failure, which is why they are often used in protective structures [8]. Ceramics, on the other hand, being brittle, tend to shatter under such conditions, with failure initiating from microcracks that rapidly coalesce. In both cases, the impact can leave behind permanent deformation and fractures, and

modelling such behaviour requires dynamic material properties that differ substantially from the quasi-static counterparts [9].

Composite materials, especially fibre-reinforced polymers, respond to high-velocity impacts in more complex and often unpredictable ways. Unlike metals, composites are anisotropic and heterogeneous, with fibres carrying most of the load and the matrix binding them together [10]. During impact, energy is dissipated through several mechanisms including fibre breakage, matrix cracking, delamination, and interfacial debonding. The direction of fibre orientation plays a crucial role in how the composite resists the incoming force. Depending on the layup and type of reinforcement, the impact might be absorbed effectively or cause catastrophic local failure without much visible damage on the surface.

One particularly challenging aspect of high-velocity impact on composites is their tendency to hide internal damage, known as barely visible impact damage (BVID), which can significantly reduce structural performance without being immediately clear. This makes the inspection and prediction of the residual strength difficult. Numerical modelling of such events often requires advanced techniques, such as cohesive zone modelling or damage mechanics to capture the initiation and evolution of different failure modes.

At the microscale, a high-velocity impact on the composites triggers a sequence of damage events that can be characterised by high strain rate-dependent behaviour of both fibre and matrix. The matrix, typically a thermoset resin, may exhibit brittle cracking under high loading rates, while fibres such as carbon or glass can undergo tensile rupture or buckling depending on the impact angle and ply orientation. Interlaminar shear stresses induced by stress wave reflections at ply interfaces often lead to delamination, which compromises the load transfer capability across the laminate. In addition, frictional heating and dynamic stress concentrations can intensify damage propagation.

2.2. Projectile Characteristics in Impact Testing

2.2.1. Study of the Projectile Type

The choice of projectile type significantly influences the outcomes of the high-velocity impact tests on composites. Soft body projectiles, such as gelatine-based synthetic birds, are often used to simulate real bird strikes because they mimic the fluid-like behaviour of biological tissue. For instance, [11] and [12] employed gelatine birds in their experiments, noting that these impactors provided accurate results comparable to real bird strikes [11], [12] Gelatine projectiles are advantageous because they replicate the dynamic deformation and energy distribution of real birds, making them a widely accepted substitute in aerospace testing.

In contrast, hard body projectiles, such as steel spheres or cylinders, are typically used to study localised damage mechanisms such as penetration or delamination. [13] used tempered steel cylinders to ensure complete energy transmission without plastic deformation of the impactor, while [14] used steel balls to investigate the micromechanical effects. Hard body impacts often result in distinct failure modes, such as fibre rupture and matrix cracking, which differ from the distributed damage caused by soft-body projectiles [15].

The debate between real birds and synthetic substitutes centres on accuracy and standardisation. While real birds provide the most realistic test conditions, their variability in size, shape, and composition makes reproducibility challenging. Synthetic substitutes like gelatine or rubber fragments offer consistency and are easier to standardise, though they may oversimplify the complex behaviour of real birds. [16] approximated bird impactors as water-based materials, which, while simplistic, yielded satisfactory results for certain applications. Approximating bird impactors as water-based materials also yields satisfactory results for certain applications.

2.2.2. Study of the Projectile Shape

The projectile geometry plays a pivotal role in the energy absorption, damage mechanism, and failure patterns of the composite laminates under high-velocity impact. Studies have

compared hemispherical, cylindrical, and blunt-nosed projectiles to determine their influence on the ballistic response of various composite configurations.

The projectile shape plays a critical role in determining the energy absorption and damage patterns in the composite materials. Blunt projectiles, such as flat-ended cylinders, cause higher energy absorption via shear plugging, a dominant mechanism in thick laminates. In one study, flat-headed projectiles induced shear plugging, accounting for up to 87% of the energy absorption in woven E-glass composites [17]. Similarly, [18] noted that blunt impactors caused the highest energy absorption due to shear-dominated failure, while conical projectiles led to more localised penetration.

Projectiles with a spherical head, often used in ballistic testing, produce a balance between the shear and tensile failure modes. Spherical projectiles were shown to produce predictable damage patterns on CFRP laminates such as petalling in thin laminates and delamination in thicker ones [19]. Similarly, [17] employed right circular cylinders which also induced petalling in the specimens.

Hemispherical projectiles, on the other hand, tend to distribute the impact energy more evenly, resulting in broader damage zones. Flat-ended and conically nosed projectiles were compared, and it was found that conical shapes required less energy for perforation in thick targets but caused more extensive deformation. Thin composites exhibited similar ballistic responses regardless of the projectile shape, whereas thick composites were more sensitive to the geometry [20].

In summary, blunt projectiles are the most effective for studying shear-dominated energy absorption. Hemispherical and cylindrical shapes are better suited for investigating distributed damage and penetration resistance. The choice of projectile shape should align with the specific research objectives, whether focusing on energy absorption mechanisms or damage tolerance. Table 2.1 summarises the differences between the projectile geometries with regards to material response and failure.

Table 2.1: Effect of projectile geometry on high-velocity impact material response and behaviour

Geometry	Dominant Failure Mode	Energy Absorption	Damage Area	Remarks
Blunt	Shear plugging	Highest	Localised	Most severe failure; used to test worst-case scenarios
Hemispherical	Mixed (delamination, cracking)	Moderate	Distributed	Balanced failure; suitable for hybrid composites
Cylindrical	Fibre rupture, petalling	Moderate–High	Distributed	Aspect ratio influences the ballistic limit and failure patterns

2.3. Material Design and Performance

2.3.1. Materials Tested

High-velocity impact testing has been performed on a wide array of materials, including metals, composites, sandwich structures, and hybrid laminates. The choice of material significantly influences not only the energy absorption capacity but also the dominant failure mechanisms, residual velocity behaviour, and overall structural resilience.

Among metals, aluminium alloys such as Al-2024 and Al-7075 are widely used in aeronautical structures due to their high strength-to-weight ratios. Under impact conditions, these materials primarily exhibit ductile failure modes, including localised tearing and petalling. When incorporated into fibre metal laminates (FMLs), aluminium provides the initial stiffness and load-bearing capacity, and although FMLs fail similarly to monolithic aluminium, they exhibit enhanced energy absorption. This is largely attributed to the synergy between the metallic and composite layers [11], [21].

Carbon fibre reinforced polymers (CFRP), composites, particularly T800S/M21 and AS4/8552 systems, are commonly selected for high-velocity impact applications. These systems offer excellent stiffness and tensile strength, but their performance under out-of-plane impact is limited due to delamination and brittle failure modes such as matrix cracking and fibre rupture [13]. Prestressing CFRPs also has a significant effect on damage behaviour. Composites under compressive preloading exhibited buckling-induced failure and reduced ballistic limits at velocities exceeding 200 m/s. Conversely, tensile preloading slightly improved the performance below 200 m/s but failed prematurely above this threshold due to amplified interlaminar and intralaminar damage [16].

In the context of structural design, sandwich panels incorporating Nomex honeycomb or flexcore (corrugated aluminium) cores with CFRP or aluminium face sheets have been shown to improve impact resistance. Ribless configurations using flexcore have been demonstrated to significantly increase the global stiffness of leading-edge panels while distributing the impact energy more evenly across the surface. This configuration also allows for simpler manufacturing and better protection of the inner structures [21].

The role of hybrid composites in impact mitigation is also prominent. Hybrid systems, such as basalt/glass, carbon/aramid, and stainless steel/acrylic combinations, have been tested to overcome the brittleness of the monolithic composites. Basalt/carbon hybrids have been observed to display superior ballistic limits compared to pure carbon fibre systems [22]. Likewise, Kevlar backings have been found to absorb 93% of the impact energy versus 77% for bonded CFRP alone. Carbon/aramid hybrids effectively delay catastrophic failure by pairing high-stiffness carbon with high-strain aramid fibres, exhibiting pseudo-ductility [19].

The stainless steel/acrylic composite system in combination with CFRP plies serves as a suitable hybrid composite system with good interfacial bonding. It achieves ductile failure through the metal phase while benefiting from the matrix toughness. Increasing CFRP layers leads to increased strength and modulus and lower strains while SSA layers increase the flexural and tensile strains. For applications where both strength and ductility are required, it may serve as a viable alternative [23].

Fibre Metal Laminates (FMLs), typically composed of alternating layers of aluminium and either glass or carbon fibres, offer a distinct advantage in bird-strike and soft-body impact scenarios. They absorb more energy than monolithic aluminium and fail in a controlled manner through a combination of shear plugging, delamination, and tearing. Researchers have supported the application of FMLs for bird-strike simulations, especially due to their layered failure mechanisms and the feasibility of strain-rate dependent modelling [11], [24].

To further improve the ductility and damage tolerance of the composites, researchers have explored tailored hybrid strategies that exploit pseudo-ductility. This is achieved either by using ultra-thin plies [25], incorporating discontinuous fibre arrays with controlled slits [26] or pairing materials with distinct strain-to-failure properties, such as carbon/aramid systems [27]. These techniques prevent sudden failure by enabling gradual fibre fragmentation or delamination, resulting in a more predictable and energy-dissipative response.

Overall, the selection and configuration of materials play a crucial role in dictating the impact response of a structure. The combination of high-modulus fibres, ductile phases, layered architectures, and smart layups, as illustrated across the cited studies, underlines the importance of material engineering in the development of next-generation impact-resistant systems.

2.3.2. Configuration of the plies

The stacking sequence, ply orientation, weave architecture, and core reinforcement strategies in the composite structures play a defining role in determining their response to high-velocity impacts. Through the deliberate design of these internal configurations, researchers have sought to enhance damage tolerance, energy absorption, and pseudo-ductility in both monolithic and hybrid composites.

One of the most critical factors influencing the impact performance is the stacking sequence of fibre plies. Placing high-strain materials such as aramid (e.g., Kevlar) on the outermost layers has been shown to significantly improve the impact resistance significantly. This configuration enables the outer layers to absorb and dissipate more kinetic energy upon

impact, thereby reducing the transmission of stresses to the interior layers. Kevlar backing vastly outperforms the carbon-only configurations with up to 93% impact energy absorption [19]. Similarly, it has been observed that placing aramid on the exterior while keeping high-stiffness carbon layers inside led to a marked improvement in the toughness modulus and ultimate strain, particularly for ply orientations aligned at 90° [27]

The weave design of the fibre layers also contributes to the interfacial bonding quality and in-plane strength distribution. Among the various patterns, the mock leno weave has emerged as particularly effective. It is formed by separating fibres mechanically to allow for small gaps simulating a leno weave pattern which is formed by twisted warp yarns. It has been reported that mock leno weave designs exhibited superior mechanical properties compared to plain or satin weaves, largely due to enhanced fibre interlocking and improved matrix wetting. This interfacial cohesion reduces delamination under high strain rates and ensures a more uniform stress transfer across the laminate [28].

In sandwich structures, reinforcement of the core plays a substantial role in damage mitigation. Tubular and corrugated core reinforcements have been investigated as alternatives to traditional honeycomb cores. In one study, sandwich panels with tubular reinforcements exhibited localised front-face damage with minimal internal or back-face delamination. Meanwhile, corrugated cores provided resistance to through-thickness failure. These reinforcement strategies are particularly effective in reducing damage in the event of soft-body or bird-strike impact scenarios [12].

The layup pattern of the hybrid plies, especially in the intercalated configurations, has also been shown to improve energy absorption. Sandwich hybrids were compared to intercalated basalt/carbon configurations, and it was observed that the latter outperformed traditional sandwich designs in terms of ballistic limit and delamination control. Intercalation of high-modulus carbon plies with ductile basalt layers enabled energy dissipation across multiple interfaces, leading to progressive damage rather than brittle failure [22]

Furthermore, the adoption of thin-ply architectures has allowed for more finely controlled damage propagation. Thin carbon plies have been observed to delay the onset of critical fibre

breakage clusters, thereby enhancing the pseudo-ductility in hybrid layups. When these thin plies are combined with high-strain materials such as S-glass or aramid, the composite not only sustains higher strains before failure but also exhibits a smoother stress-strain response, which is particularly advantageous for crashworthiness [25].

In summary, the internal architecture of composites including ply stacking, fibre orientation, weave type, and core reinforcement has a profound impact on how these materials respond under high-velocity impact. The outer-layer positioning of ductile fibres, intercalated stacking, mock leno weave patterns, and core reinforcement all contribute to mitigating damage and extending the functional life of impact-prone composite structures.

2.3.3. Orientation of the plies

The orientation of fibres within a composite laminate is a fundamental factor influencing how damage initiates and propagates under high-velocity impact. Fibre direction dictates the path of least resistance for crack growth, the stiffness and strength in various directions, and the extent of interlaminar versus intralaminar damage.

In unidirectional composites, impacts along the fibre direction (0°) typically result in fibre rupture and minimal delamination, as the load is carried directly by the high-strength fibres. However, when impacts occur transverse to the fibre direction (90°), the matrix bears more of the load, leading to greater delamination and matrix cracking due to its comparatively low strength and toughness. This directional sensitivity in carbon/aramid hybrid laminates is highlighted in [27]. Specimens with 90° carbon plies in the mid-plane exhibited significantly higher failure strain and toughness modulus than compared to those oriented at 45°. This suggests that the damage tolerance improves when fibres are aligned perpendicular to the expected impact direction, as the energy is more evenly distributed through the thickness.

In addition, multidirectional layups, which include ±45°, 0°, and 90° orientations, are often employed to balance in-plane properties and delay the onset of catastrophic failure. [16] used a layup of 23 unidirectional CFRP plies in a $[45/0/45/90/45/0/(45)_2/(0)_2/45/90]_S$ stacking

sequence, showing that mixed orientations promote a more progressive damage evolution, involving both interlaminar delamination and intralaminar cracking. This complex failure mode enhances the energy absorption capability of the laminate, especially in high-velocity events where both tensile and shear stresses are present.

Moreover, in woven fabrics, fibre crimp and crossovers introduce local stress concentrations that affect damage progression. [29] found that plain-woven Kevlar exhibited delayed stress distribution and less effective impact resistance compared to multiaxial or unidirectional laminates, largely due to the fibre undulation inherent in the weave. This demonstrates that not only the orientation but also the type of fibre architecture affects how damage propagates under impact.

In summary, fibre direction strongly controls the damage mechanisms in composite laminates. Axial fibre alignment enhances strength but limits energy dissipation, whereas off-axis and multidirectional layups facilitate delamination and matrix shear.

2.3.4. Manufacturing method

The manufacturing method of the composite materials directly affects their impact performance by influencing the void content, fibre alignment, resin distribution, and interfacial bonding. Processes such as vacuum-assisted resin infusion moulding (VARIM), autoclave curing, and confinement pressing are commonly used in the fabrication of both monolithic and hybrid composites.

Vacuum infusion techniques, such as VARIM, offer the advantage of producing low-void content laminates with controlled fibre volume fractions. Researchers have employed VARIM to manufacture hybrid laminates involving carbon, aramid, and glass fibres [27], [30]. The success of these methods in achieving consistent mechanical properties depends heavily on maintaining a stable vacuum pressure during infusion and cure, which helps avoid internal defects and ensures strong interfacial adhesion between dissimilar fibres.

Autoclave curing, used in works such as [22] provides a high-quality finish and superior consolidation, especially for aerospace-grade CFRPs. It allows precise control of temperature and pressure, which is critical for resin flow, ply compaction, and achieving the desired laminate thickness. Although costlier, autoclave processing remains the standard for high-performance components such as aircraft skins, flaps, and leading edges.

One particularly severe condition tested in both experimental and numerical studies involves the combination of compression preloading and blunt impact. Compression preloading simulates in-service structural states such as aerodynamic loading or thermal expansion forces. When a structure under such preloading is subjected to a blunt-nosed projectile, the resulting damage is significantly more severe. The compressive load leads to instability-induced failures such as local buckling, while the blunt impact induces shear plugging and deep matrix damage [15][12][5]. The ballistic limit under this combined condition is often lower than that in the unstressed case where prestressed panels exhibit earlier onset of both interlaminar and intralaminar failure modes [16].

In terms of structural vulnerability, leading edges and control surfaces such as flaps are high-risk zones in aircraft structures. These regions are most exposed to foreign object impacts such as bird strikes during take-off and landing. Damage in these zones is characterised by high local deformation, extensive delamination, and, in some cases, complete skin rupture [21], [31]

2.4. Experimental Testing Methodologies

The study of high-velocity impact behaviour in composite materials relies heavily on well-controlled and repeatable experimental testing methods. A range of projectile launch systems, target configurations, and measurement techniques are used to simulate real-world conditions.

Among the most used launch mechanisms are pneumatic cannons, gas guns, and air guns capable of delivering projectiles at velocities exceeding 100 m/s. [21] used a pneumatic

cannon to simulate bird strike conditions on aeronautical sandwich panels, achieving impact velocities in the range of 129–140 m/s. Single-stage gas guns have been employed to test composite panels under impact velocities ranging from 100 m/s up to over 400 m/s[13], [21], [32]. These methods offer consistent acceleration of projectiles and precise control over the impact energy.

Given the impracticality and ethical concerns of using real birds in testing, various surrogate projectiles have been adopted. Among the most realistic are gelatine birds, used in studies such as those by [11] and [12], which replicate the soft-body, water-rich behaviour of bird impacts. Other substitutes include steel and glass spheres which offer repeatable mass and geometry while ensuring clean, quantifiable impact signatures [13], [32].

To accurately measure the impact velocity, researchers commonly use photoelectric sensors or high-speed cameras. A gate of two photoelectric cells is placed between the gun and specimen to measure the projectile velocity before impact, offering a simpler and more cost-effective alternative to high-speed imaging [13]. When more detailed analysis, such as the tracking of deformation modes or crack propagation, is required, high-speed video cameras are employed.

Strain gauges are another critical component of the experimental setup. In many cases, they are affixed to the rear face of the composite panel to measure the strain-time history, detect through-thickness stress propagation, and validate numerical simulations [15]. A dual approach of strain gauge application with residual velocity measurements leads to a more robust monitoring system for such high-impact scenarios [33].

Although full-scale testing provides the most representative results, it is often expensive and time-consuming. As a result, coupon-level testing has become a practical substitute. [11] specifically noted the effectiveness of coupon tests, provided they are properly validated against full-scale data. These tests enable material screening, layup optimisation, and damage mode analysis under controlled conditions before scaling up to structural components such as wing leading edges or fuselage skins.

In conclusion, the experimental impact testing combines high-velocity launch systems with realistic soft-body or rigid projectiles and advanced instrumentation to characterise material behaviour. The integration of coupon testing, surrogate birds, and precise velocity measurement ultimately assists in informing the design of safer and more resilient aerospace structures.

2.4.1. Study on the varying impact velocities:

A critical dimension in understanding the high-velocity impact behaviour of composites is the study of the impact velocity range, which governs not only the nature of the damage but also the underlying failure mechanisms, strain-rate sensitivity, and structural response. Across the literature, experimental and numerical investigations have examined velocity ranges spanning from as low as 43 m/s to as high as 566 m/s, depending on the application, material type, and projectile used.

Most research focusing on bird strike scenarios centres on the velocity range of 100 to 200 m/s. For instance, [16] evaluated flat composite panels and leading-edge structures using impact velocities of 100, 150, and 200 m/s. Similarly, [21] used velocities in the 129–140 m/s range with dummy birds to simulate real-world airframe impacts. [31] considered even higher values (145.7, 200, and 280 m/s) to explore both Lagrangian and Eulerian modelling strategies for flap and leading-edge structures.

As the velocities increase beyond 200 m/s, the nature of the failure changes significantly. In prestressed laminates, higher impact velocities tend to amplify both interlaminar and intralaminar damage, leading to an earlier failure onset. Prestressed CFRP panels, while performing slightly better under tension at lower velocities (<200 m/s), exhibit reduced ballistic limits and greater delamination at velocities above 200 m/s due to the strain energy compounding with the external kinetic load [16].

Material-specific ballistic limits also emerged as a key metric in these studies. [13]reported a ballistic limit of 130 m/s for a woven carbon/epoxy laminate tested with steel cylindrical projectiles. Beyond this velocity, the laminate experienced full perforation and severe fibre

and matrix damage. Other materials, such as basalt/carbon hybrids [22] and Kevlar-reinforced systems [19], demonstrated higher ballistic thresholds due to their enhanced energy absorption capacity and more progressive failure modes.
At the upper end of the velocity spectrum, [20] explored impact velocities up to 566 m/s using hardened steel projectiles on E-glass reinforced plastics. These extreme conditions are more representative of ballistic or debris impact scenarios and are essential for validating material performance in defence and high-speed aerospace applications.

In summary, the impact velocity not only dictates the extent and type of damage in composite materials but also determines the validity of numerical modelling strategies (e.g., Lagrangian vs. Eulerian), the necessity of strain-rate sensitive models, and the relevance of structural preloading. Research consistently shows that while most design-relevant impacts occur in the 100–200 m/s range, careful consideration must be given to both lower and higher velocity regimes to fully characterise material behaviour across operational extremes.

2.4.2. Failure modes

Carbon fibres typically fail through brittle fracture with minimal energy absorption, leading to sudden structural degradation. This brittle behaviour is evident in pure CFRP laminates where localised fibre breakage and limited matrix deformation dominate the damage modes [16], [32]. In contrast, ductile fibres such as basalt and aramid exhibit significant fibre stretching and plastic deformation before rupture, which enables higher energy dissipation and damage tolerance [22], [27].

Hybrid composites aim to balance these behaviours. For instance, [22] reported that intercalated basalt-carbon hybrids exhibited higher ballistic limits (V_{50}) than pure CFRP, owing to the ductile response of the basalt layers and increased delamination, which enhanced the energy dissipation. However, this also introduced higher interfacial stress concentrations. [33] showed that while hybrid glass/carbon laminates outperformed pure carbon in impact resistance, they suffered from increased delamination at the glass-graphite interfaces.

Delamination and fibre rupture remain the dominant failure modes in such hybrids, particularly under through-thickness loading [12]. The interface quality, ply orientation, and stacking sequence significantly influence the damage mechanisms. To promote pseudo-ductile behaviour and delay penetration, placement of glass or aramid layers on the exterior proves to be a viable solution [17], [27]

2.5. Numerical Modelling and Simulation

High-velocity impact modelling of composite structures requires accurate numerical approaches to capture complex failure mechanisms, strain-rate dependencies, and projectile-target interactions. Several FEM techniques and simulation strategies have emerged, each with specific advantages and limitations. Prominent software used for high-velocity impact simulation includes LS-DYNA, ABAQUS/Explicit, and ANSYS/Explicit. These solvers support large deformation analysis, advanced contact interactions, and dynamic failure modelling necessary for simulating ballistic events.

The Lagrangian method is widely used because of its computational efficiency and the availability of complex material models. It performs well at impact velocities below 150 m/s, beyond which mesh distortion becomes severe and leads to numerical instability [31]. Nonetheless, [21] identified it as the most accurate approach overall for structural response prediction, despite the risks of instability under extreme deformation.

SPH is highly suited for projectile modelling, especially when simulating soft body impacts such as bird strikes. It captures the fluid-like deformation of birds accurately and avoids mesh distortion altogether. [21] recommended SPH specifically for modelling deformation behaviour of the bird while modelling the structural parts in the Lagrangian formulation. [16] and [34] also supported SPH–FEM coupling for improved realism in bird strike simulations.

CEL excels at very high velocities (>150 m/s), especially when modelling fluid-structure interaction. It prevents mesh distortion by representing the projectile as a material flowing through a fixed mesh. [16] showed that CEL provides better accuracy than Lagrangian for soft-

body projectile impacts, particularly when the deformation and spread of the projectile are significant. [35] concluded that CEL is the most robust method for bird modelling, with Lagrangian being viable only up to moderate velocities.

Accurately modelling strain-rate sensitivity is critical for high-velocity impact simulations. [14] introduced the MicroRate model, a micromechanics-based multi-scale framework that significantly improves the simulation fidelity by accounting for the rate-dependent damage evolution. The results showed strong agreement with the experimental ballistic limits and failure modes. [24] emphasised the need to include anisotropic strain rate effects, particularly in composite laminates, using a continuum damage mechanics (CDM) approach. This helps predict localised failure more realistically under dynamic loading.

Delamination is a dominant failure mode in composites during impact. Ply-level modelling using stacked shells with cohesive elements is recommended to capture both intra- and inter-laminar damage [16]. This method offers a balance between the computational cost and the failure accuracy. Damage propagation can be validated using residual velocity comparisons [13] or DCB/ENF derived traction-separation laws [32].

The residual velocity of the impactor remains one of the most reliable parameters to validate numerical models [13]. Damage mode comparison (delamination, fibre rupture, core crushing) with experiments is also widely used. [21] successfully validated a full-scale model using only a single experimental test, demonstrating the potential of efficient modelling when aligned with appropriate validation metrics.

Among the various FE modelling strategies, a Lagrangian approach is optimal for the structure when the velocities remain moderately high. For ultra high-velocity bird strikes, a CEL or SPH–FEM hybrid model offers the best accuracy for projectile behaviour. Strain-rate effects, cohesive elements, and proper validation metrics such as residual velocity must be included to enhance fidelity [14], [16], [21], [24]

3. METHODOLOGY

This chapter presents the methodology adopted to investigate the high-velocity impact behaviour of CFRP–PET foam sandwich panels. It integrates both the experimental campaign, where specimens were subjected to controlled impacts using a pneumatic gas gun, and the numerical modelling, where finite element simulations were carried out in Abaqus/Explicit to reproduce and interpret the observed behaviour.

3.1. Experimental Campaign

The experimental campaign was designed to evaluate the high-velocity impact response of carbon-fibre reinforced polymer (CFRP)–polyethylene terephthalate (PET) foam sandwich panels. The methodology was structured to ensure transparency and reproducibility, covering specimen fabrication, preparation for testing, and the gas-gun impact procedure.

3.1.1. Materials

This section describes the materials used in the construction of the sandwich panels later presented in this work. Three different constituent materials were selected: two types of carbon fibre reinforcements and a polymeric foam core: i) Carbon Fibre Plain Weave (195 g/m², 0/90°), ii) Carbon Fibre Multiaxial CBX 100 (±45°), and iii) Airex® T92.60 Structural Core

The Carbon Fibre Plain Weave consists of T700 fibres oriented in 0° and 90° directions. This fabric is commonly employed in aerospace and high-performance applications due to its high in-plane stiffness and strength, combined with balanced behaviour in orthogonal directions. Its woven architecture provides good surface stability and damage tolerance under impact.

The Carbon Fibre Multiaxial CBX 100 is a biaxial multiaxial fabric composed of T700 12K carbon fibres arranged at ±45°, with an areal density of 100 g/m² and a nominal thickness of 0.15 mm. The ±45° orientation enhances the shear properties of the laminate and contributes to energy

dissipation under out-of-plane loads. This reinforcement is compatible with epoxy, vinyl ester, and polyester resin systems.

The Airex® T92 is a closed-cell recyclable PET foam widely used as a structural core in sandwich composites. In this work, the selected grade has a thickness of 5 mm and a density of 60 kg/m³. The T92 core combines low density with high specific stiffness, good fatigue performance, and thermal stability, making it suitable for aerospace and marine applications. Its cellular structure also improves energy absorption and impact resistance.

The mechanical characterisation of the carbon fibre reinforcements was carried out in a previous experimental campaign at the University of Minho [36] where standardised testing was performed in accordance with ASTM guidelines. Mechanical properties were experimentally determined through: ASTM D3039/D3039M-14 – tensile properties, ASTM D7264/D7264M-15 – flexural properties, and ASTM D3518/D3518M-13 – in-plane shear properties.

Table 3.1 summarises the average properties of the constituent materials. The values for the carbon fibre fabrics correspond to the experimental characterisation performed according to ASTM D3039, D7264 and D3518, while the properties of Airex® T92 are taken from the manufacturer's datasheet.

It should be noted that the tensile and flexural tests of Carbon Fibre Multiaxial CBX 100 were performed along the 0° axis of the specimen, while the carbon fibres were oriented at ±45°. As a result, the values obtained are dominated by the shear response of the laminate and cannot be directly compared with the results of the plain weave 0/90° fabric

Table 3.1: Nominal properties of constituent materials

Material	Density (g/cm³)	Tensile Strength (MPa)	Tens. Modulus (GPa)	Flexural Str. (MPa)	Flex. Mod. (GPa)	In-plane Shear Str. (MPa)	Shear Mod. (GPa)	Orie-nt-ation	Areal Wt. (g/m²)
Carbon Fibre Plain (195)	~1.77	~480	~42	~486	~766	~74	~4.8	0/90°	195
Carbon Fibre CBX 100	~1.77	~156	~7	~164	~154	62	~7.5	±45°	100
Airex® T92 (PET foam)	0.06	1.5	0.085	-	-	0.55	0.015	–	–

3.1.2. Specimen Design and Preparation

The sandwich panels consisted of two CFRP face sheets bonded to a PET foam core. Each face sheet was composed of two commercial laminates: Rebelco 196 (plain weave) and Rebelco CBX 100 (quasi-isotropic). The core material was Airex T92.60 PET foam, with a nominal density of 60 kg/m³ and a thickness of 5 mm. The matrix system used was SR1280/SD4775 epoxy resin.

The layup sequence was as follows:

1. Carbon fibre plain weave (195 g/m²)
2. Carbon fibre CBX (100 g/m²)
3. Airex T92 PET foam core (5 mm, 60 kg/m³)
4. Carbon fibre CBX (100 g/m²)
5. Carbon fibre plain weave (195 g/m²)

Nine sandwich specimens were manufactured by TEKEVER, a leading Portuguese company in the design and production of unmanned aerial vehicles, using vacuum infusion. After curing, each specimen was measured to verify dimensional consistency. Table 3.3.2 presents the mean dimensions and coefficient of variation (COV) across all specimens.

Table 3.3.2: Mean Specimen Dimensions and Thickness

Parameter	Mean [mm]	COV [%]
Length	308.5	1.3
Width	308.4	1.3
Thickness	6.02	1.3

The low COV values (< 0.02%) confirm a high level of manufacturing consistency, minimizing variability in subsequent impact results.

Each specimen was prepared for Digital Image Correlation (DIC) by first applying a white primer coat, followed by a layer of epoxy resin and finally spraying granite paint while the epoxy was still wet. This procedure yielded a high-contrast speckle pattern, optimally suited for digital image correlation (DIC) and precise optical tracking. The ink particles were embedded within the epoxy layer and securely bonded to the surface of the CFRP–PET plate, ensuring the pattern's integrity throughout the impact event. By anchoring the speckle particles to the plate, this approach effectively prevents speckle displacement or projection during testing. Figure 3.1 presents the sequential application steps—including primer, epoxy, and final speckle pattern—along with the resulting DIC-ready plate surface.

(a) (b) (c)

Figure 3.1: Speckle-pattern application setup using primer, resin, and granite spray. (a) Application of epoxy layer after primer; (b) Plate after DIC pattern application; (c) Detail of DIC pattern.

3.1.3. Experimental Setup

Specimens were marked at the centre with a fine marker to ensure accurate projectile alignment. They were mounted in a rigid metallic clamping frame, secured with eight strips of duct tape along the edges, and the frame was bolted to guarantee flatness and immobilisation during testing. Figure 3.2 shows the metallic clamping fixture and cameras setup anda specimen fixed pre-impact.

(a) (b)

Figure 3.2: (a) Metallic clamping fixture with cameras. (b) Specimen fixed to fixture pre-testing

The projectile used was a hardened AISI 4340 steel sphere, with a diameter of 19.05 mm, mass of 28.05 g, density of 7.85 g/cm³, and tensile strength of 745 MPa. To stabilise the projectile in the launch barrel, it was positioned inside a foam sabot, lightly taped to prevent displacement prior to firing. The projectile and sabot are illustrated in Figure 3.3 while the velocity measurement arrangement is shown in Figure 3.4.

Figure 3.3: Projectile foam sabot and AISI 4340 alloy steel projectile

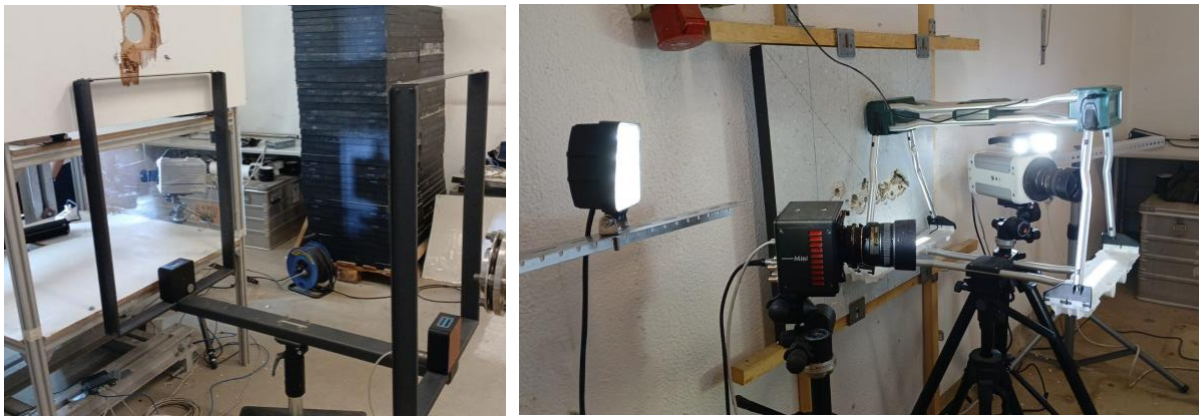

Figure 3.4: IR gate for impact velocity measurement and high-speed camera setup

The projectile was loaded into impacts were carried out with a single-stage pneumatic gas gun. The system consisted of a 4.0 m-long launch barrel connected to a pressurised chamber. After loading the sabot and projectile, the chamber was sealed and pressurised to 1.4 bar. Upon release, the projectile was accelerated through the barrel towards the target. Velocity was measured using infrared (IR) photogates positioned at the barrel exit. A high-speed camera system was synchronised with the DIC software to capture both projectile motion and specimen deformation. Lighting was adjusted to avoid glare and ensure clear image acquisition. The complete gas-gun arrangement is presented in Figure 3.5.

Figure 3.5: Gas gun test setup with 4-meter-long funnel

The funnel consisted of a sabot docking mechanism at the far end. The funnel was connected with an air compressor which supplied air from outside. Moreover, the complete setup was connected with a controller and data acquisition system in a separate room. These allowed for manual launch and acquiring instant high-speed camera imaging. A complete schematic of the test setup is shown in Figure 3.6.

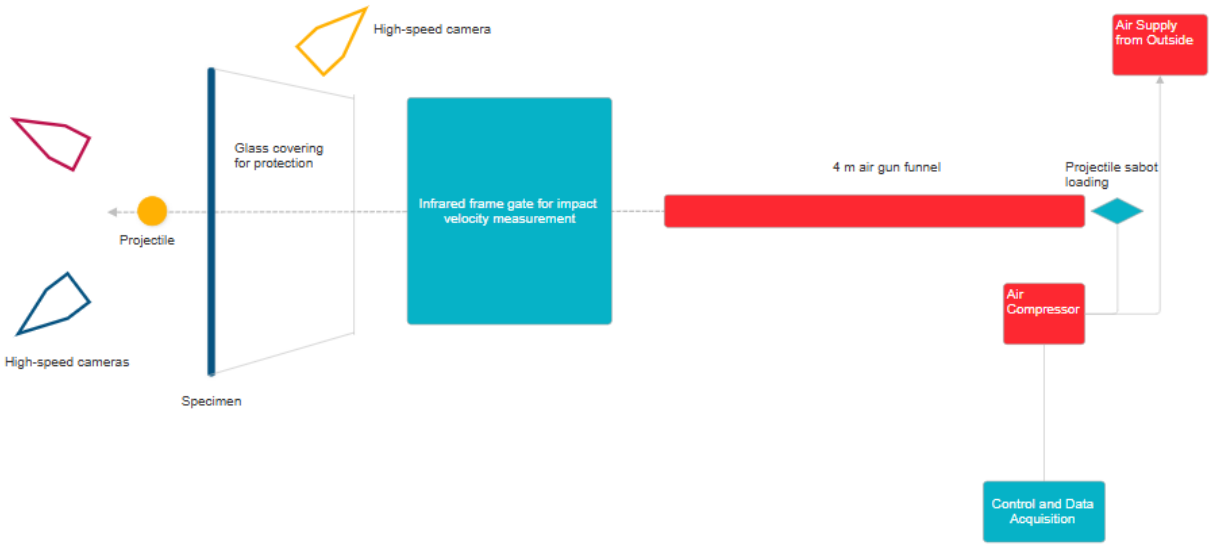

Figure 3.6: Top-down view schematic of the experimental setup

3.1.4. Test Matrix

A total of nine specimens were tested across four target impact velocities: 55.9, 80.0, 136.3, and 197.8 m/s. The measured impact velocities for each specimen are listed in Table 3.3. For each velocity group—referred to as Test Series IV-50, IV-80, IV-130, and IV-190—two specimens were tested to verify repeatability, except at the highest velocity, where only one specimen was assessed. Selecting these velocity levels allowed for a systematic investigation of how failure mechanisms evolve as impact energy increases. Specimens were grouped by Test Series for straightforward identification, with the series labels corresponding to the recorded impact velocities.

Table 3.3.3: Impact velocity measured for each specimen tested.

Specimen	Impact Velocity (m/s)	Test Series	Impact Velocity (m/s)
01	56.03	IV-50	55.9 (0.29%)
02	56.03		
03	56.00		
04	55.69		
05	82.01	IV-80	80.0 (3.49%)
06	78.05		
07	135.59	IV-130	136.3 (0.76%)
08	137.06		
09	197.80	IV-190	197.8 (n.a.)

Note: the value between parenthesis corresponds to the coefficient of variance.

3.2. Numerical Modelling and Simulation

Finite element modelling (FEM) was conducted in Abaqus/Explicit to reproduce the high-velocity impact response of the CFRP–PET foam sandwich panels. The modelling approach was developed in three progressive stages: a baseline metallic panel model, an isolated foam core model, and the complete sandwich panel model. This incremental procedure allowed systematic verification of modelling assumptions and facilitated the treatment of the foam's complex behaviour. For clarity, the three-stage modelling strategy is schematically

represented in Figure 3.7, highlighting the incremental progression from simple validation models to the full sandwich panel model employed for comparison with the experimental campaign.

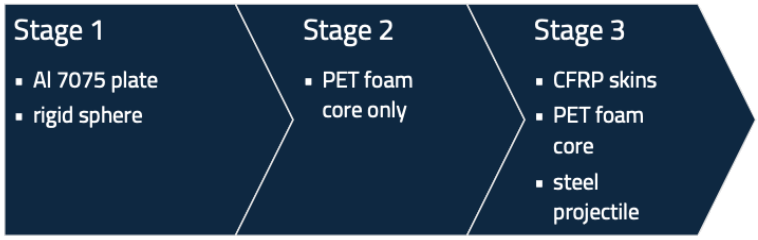

Figure 3.7: Three-stage modelling strategy highlighting incremental progression

For the first phase, a simple high-velocity impact model was defined using a metallic specimen Aluminium 7075 of similar dimensions and a discrete rigid body of infinite stiffness at a velocity of 500 m/s. Once a basic impact setup was established, an isolated foam core model was implemented where there were no facesheets involved. This was carried out to model the complex foam behaviour without complications before implementing the facesheet and core interactions. The modelling of the foam's dynamic behaviour resulted in numerous errors and instabilities that are discussed later in Chapter 4. A visualization of the Von Mises stress fields for both the above setups is shown briefly in Figure 3.8.

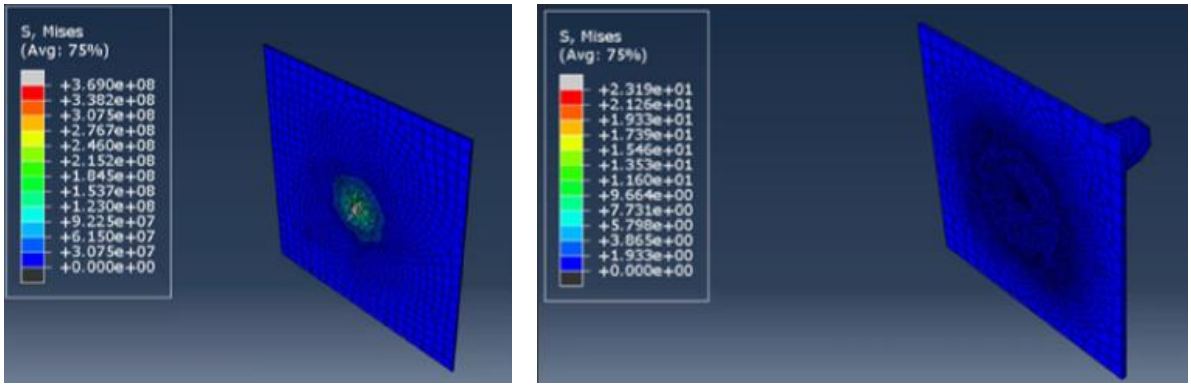

(a) (b)

Figure 3.8: Impact simulation of (a) discrete rigid 19mm projectile on Al 7075 panel at 500m/s and (b) discrete rigid 19mm projectile on Airex T92 foam core at 60 m/s

Finally for the last stage, a complete three-dimensional FEA model was implemented with the core, face sheet, and projectile modelled as independent bodies. 3D deformable solid elements were used for the foam core while conventional shell elements were used to model the CFRP skins of 300 mm x 300mm dimensions each. The projectile was also modelled as a 3D solid deformable sphere of 19.05 mm diameter.

The conventional shell CFRP skin part was then assigned 4 plies of 0.1 mm thickness each in the Composite Layup Manager with the orientation 0°/90°/45°/-45° with three integration points each. The two skins on either side are instance copies of each other. The properties for the CFRP are tabulated in Table 3.4. Note that the fracture energies are set to minimum. The scope was to capture the general behaviour of the impact. Since, the experimental specimens failed at all velocities, the specified fracture energies allowed to capture the general behaviour with reduced computational cost.

Table 3.4: Properties of the CFRP in the numerical model

Density (kg/mm^3)			1.7E-06					
Elastic Properties								
E1 (MPa)	**E2 (MPa)**	**E3 (MPa)**	**Nu12**	**Nu13**	**Nu23**	**G12 (MPa)**	**G13 (MPa)**	**G23 (MPa)**
65000	10000	10000	0.3	0.3	0.45	5000	5000	3700
Hashin Damage								
X_t (MPa)	X_c (MPa)		Y_t (MPa)	Y_c (MPa)		S_L (MPa)	S_T (MPa)	
900	700		50	180		90	90	
Hashin Damage Evolution								
G_{ft}	G_{fc}		G_{mt}	G_{mc}		G_L	G_T	
0	0		0	0		0	0	

A general explicit hard body contact algorithm is used to model all interactions in the model. This includes the panel-projectile interactions and the contact between skin and core. Moreover, a Tie constraint was applied between the core and skins simulating complete

adhesion. The panel is constrained at the edges by applying the Encastre Boundary Condition simulating real-life robust fixation of the panel in the frame. The projectile velocity is defined as a predefined field in the Initial step in the negative Z-axis direction. All other translational and rotational velocities are constrained to avoid deviation from centre. The impact step is defined under General, Explicit with a time period of 15 ms which is relative to the approximate impact time period of 11 ms from launch under the experimental conditions.

In most literature, the model for the face-sheets and the core uses a built-in vectorized used material subroutine known as VUMAT. The PET foam is especially complex to model due to its dynamic non-linear behaviour. In Abaqus, such semi-rigid foams are modelled under Crushable Foam. The validity of PET foam modelling under Crushable Foam has been validated under various arrangements and conditions. However, the Crushable foam model cannot simulate damage evolution as it does not account for element deletion. It is not feasible to model impact fracture and fragmentation alone using this pre-defined model. For this reason, a Tsai-Wu failure criterion is implemented in conjunction with the Crushable Foam to simulate element deletion. This is further implemented using a VUMAT subroutine known as VUSDFLD [37]. However, under the scope of the current work, no user-defined subroutine was employed. A Crushable foam model in conjunction with a Ductile Damage Evolution model was employed for simplification. Moreover, the strain rate independence for the PET foam impact response was assumed. This assumption has been shown to be valid for the dynamic foam behaviour [38]. The properties of PET foam core used are tabulated in Table 3.5.

Table 3.5: Properties of PET foam core in the numerical model

Density (kg/mm^3)		6E-08	
Elastic Properties			
Young's Modulus (MPa)	**Poisson's ratio**		
45	0.3		
Crushable Foam			
Compression Yield Stress Ratio		**Hydrostatic Yield Stress Ratio**	
1.2		3	
Ductile Damage			
Fracture Strain	**Stress Triaxiality**	**Strain Rate**	**Displacement at Failure**
0.25	0	0	0.4

The mesh was refined in the impact zone relative to the rest of the panel for computational cost efficiency. A circular partition in both facesheets and core centre was replaced by a square partition of dimensions 126 mm x 126 mm to allow for a more structured mesh. A mesh element size of 15 mm and 2 mm was defined for the part globally and for the local impact zone respectively. Element deletion was enabled with maximum degradation at 0.9. The element type for the core was reduced integration, hexahedral elements of linear order while for the facesheets shell, quadrilateral elements of linear order were implemented. The meshed pattern for facesheets and core is shown in Figure 3.9

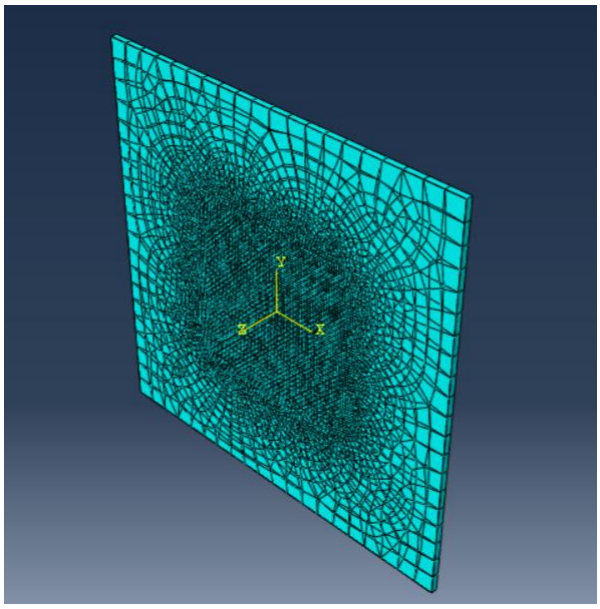

Figure 3.9: Mesh pattern for the model

The model was designed to be validated against experimental data by comparing residual projectile velocities, observed damage modes (perforation, delamination, and matrix cracking), and stress field propagation. Direct validation using strain-field measurements from Digital Image Correlation (DIC) was not performed due to time constraints but is identified as an essential direction for future work.

THIS PAGE WAS INTENTIONALLY LEFT BLANK.

4. RESULTS AND ANALYSIS

4.1. Experimental Results

4.1.1. Post-impact damage observations

Macroscopic post-impact inspections revealed that the CFRP–PET foam sandwich panels failed by complete perforation across all tested velocities. However, the size, morphology, and localisation of the damaged zones varied significantly with impact velocity. Representative specimens are shown in Figure 4.1-Figure 4.4.

At the lowest velocity of 55.9 m/s, surface damage included local cracking at the impact point and minor paint delamination. The projectile completely perforated, and the cracking seemed to align preferentially with the composite weave path. The measured diameter of the damaged region was almost double that of the projectile indicating substantial and localized surface disruption. An example is shown in Figure 4.1.

Figure 4.1: Post-impact damage at 55.9 m/s

At moderate velocities of 80 m/s, specimens exhibited visibly larger damage zones. Paint layers detached and fibre breakage became more apparent. Some specimens maintained relatively compact damage areas, likely due to better adhesion from rougher surfaces or more uniform resin coverage. A representative example is shown in Figure 4.2

Figure 4.2: Post-impact damage at 80.0 m/s.

For high-velocity impacts at 136.3 m/s, full perforation was consistently observed like the previous velocities. The projectile passed entirely through the specimens leading to fibre breakage and matrix cracking in the centre. The foam core was exposed in multiple cases confirming through-thickness failure. The entry and exit points often exhibited fibre pull-out and irregular delamination patterns. Figure 4.3 shows the post-impact damage for such a specimen at 136.3 m/s.

Figure 4.3: Post-impact damage at 136.3 m/s.

At the highest velocity of 197.8 m/s, the projectile passed cleanly through the specimen with minimal deformation or expansion around the hole. The impact speed was too great for the composite to absorb significant energy resulting in a narrow, clean penetration path. The damage is depicted in Figure 4.4.

Figure 4.4: Post-impact damage at 197.8 m/s

Overall, these observations suggest that the CFRP–PET sandwich configuration exhibited limited energy absorption capacity, with failure dominated by perforation even at the lowest

tested velocity. Increasing impact velocity primarily influenced the extent of delamination and fibre breakage, while the fundamental failure mode remained unchanged.

4.1.2. Residual velocity calculations

The residual velocity of the projectile following impact is a key parameter used to assess the energy absorption capacity of the specimen. To determine this, high-speed camera footage was analysed with the PFV4 software, enabling frame-by-frame examination of the projectile's movement. By referencing the known frame rate of 9,000 frames per second, the time interval between consecutive frames was established, allowing the calculation of the apparent distance traversed by the projectile in footage from both cameras. This provided an apparent velocity measurement.

Subsequently, trigonometric analysis was applied to derive the actual velocity, taking into account the geometric arrangement of the cameras and the angle of projectile travel relative to each camera's line of sight. The experimental setup, depicted schematically in Figure 4.5 assumes that both cameras and the projectile maintain a planar alignment, and that any vertical deflection from the central axis is negligible. This approach facilitates a precise determination of the projectile's residual velocity post-impact for further energy dissipation calculations.

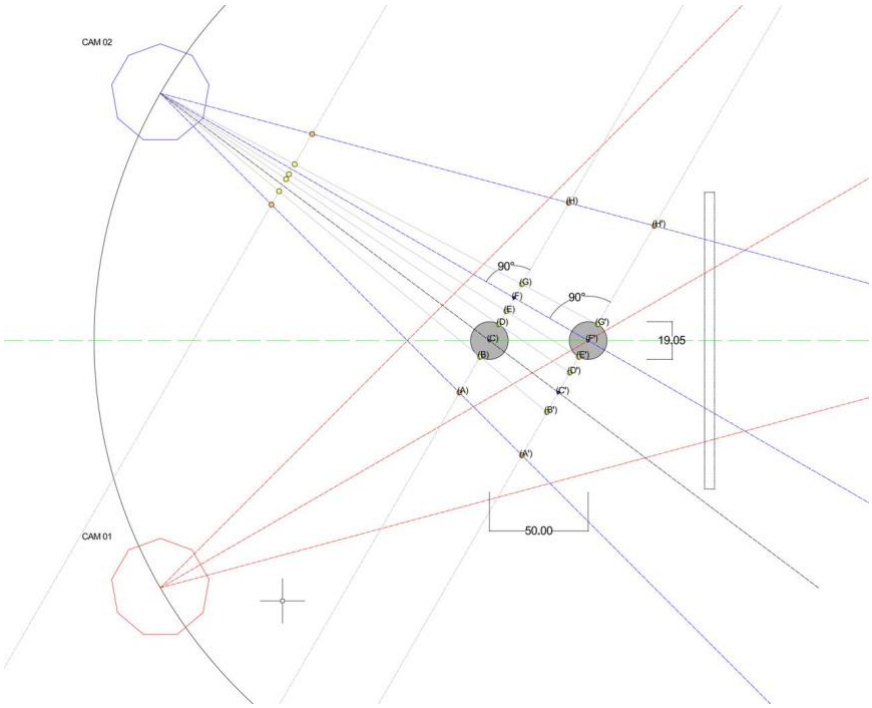

Figure 4.5: Top view schematic of the positions of the projectile post-impact and the two cameras assuming no horizontal deflection i.e. projectile is symmetric w.r.t. both camera angles

Where CAM01 and CAM02 are the positions of the two cameras. BD is the apparent diameter measured from CAM 02, CF' is the actual distance travelled by the projectile from initial to final position while CF is the apparent distance as measured by CAM 02. A relation can be established between the real diameter 19.05 mm and the apparent diameter BD and the apparent and real distances as shown in Eq. 5.1.

$$Real\ distance\ CF' = \left(\frac{19.05}{BD}\right) \times \left(\frac{CF}{\sin\theta}\right) \tag{1.1}$$

Where θ is the angle between the projectile and the CAM 02 (30 degrees in the above image).

In case of a second scenario where the projectile is not symmetric with the two cameras and rather it deviates from the centre of axis, the new relation is considered with an additional angle α along with θ. It is either added or subtracted from θ depending on the camera position. The Figure 4.6 shows a schematic for asymmetric projectile movement.

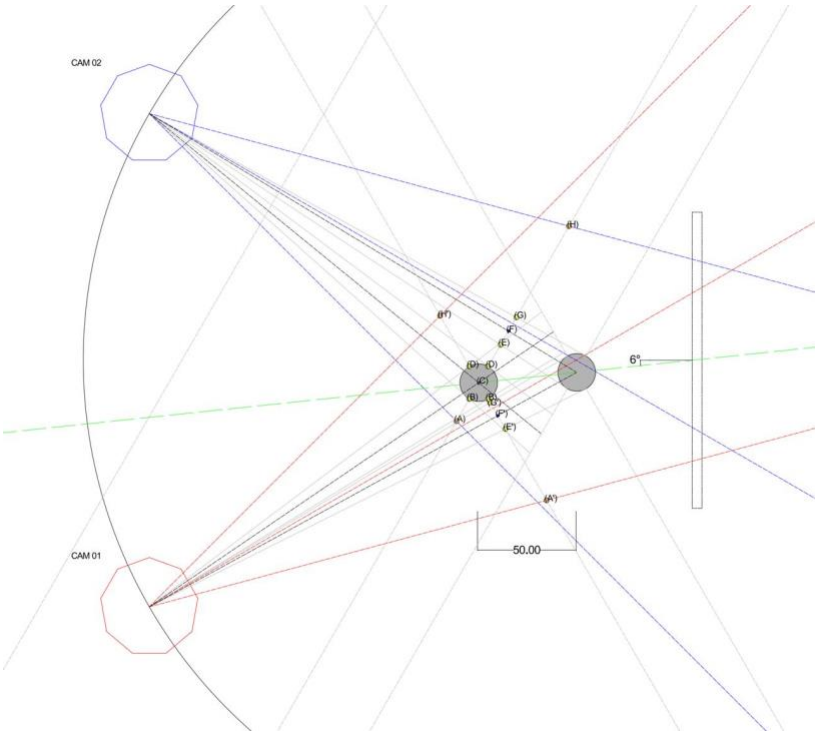

Figure 4.6: Top view schematic of the positions of the projectile post-impact and the two cameras assuming slight horizontal deflection i.e. projectile is asymmetric w.r.t. both camera angles

In the above figure, the projectile deviates by an angle α of 6° (assumed for the purpose of illustration). This deviated angle α can be calculated. We know that the real distance measured from the CAM 01 and CAM 02 is equal in magnitude. By virtue of this fact, we can solve for α by equating the two equations:

$$\left(\frac{19.05}{BD_1}\right) \times \left(\frac{CF_1}{\sin(\theta + \alpha)}\right) = \left(\frac{19.05}{BD_2}\right) \times \left(\frac{CF_2}{\sin(\theta - \alpha)}\right)$$

Where BD_1 and BD_2 are the apparent diameter and CF_1 and CF_2 are the apparent distances travelled by projectile from CAM01 and CAM02 respectively.

By solving for this equation, we get α and can then calculate the real distance using either of the above two equations. It is important to emphasize that, beyond the trigonometric relationships previously detailed, additional factors such as camera lens distortion and image scaling significantly influence the accuracy of measured projectile velocities. Notably, the apparent diameter of the sphere, as observed in the initial and final frames, may vary due to these optical effects. Such variations directly impact the calculation of apparent displacement and, consequently, the determination of residual velocity. To address this, the average of the

measured diameters at the relevant frames was used in the analysis, and the associated error margins are reported in Table 5.1. This approach ensures that the calculated results more accurately reflect the true dynamics of the projectile motion under investigation.

To determine the apparent diameter and distances, the Measurement tool in PFV4 was utilized. A specific time frame was selected for both cameras where the diameter of the projectile at the first frame and last frame was calculated and the mean taken. Furthermore, the apparent distance was also calculated by drawing straight lines from centre of each projectile at the initial and final instants defined. If the apparent distances were equal for both cameras, then the symmetric condition was considered while in case of discrepancy between apparent diameters, the asymmetric scenario was considered and α calculated using the Microsoft Excel's Solver tool. Figure 4.7 shows the manual measurement of the apparent diameters and distances for CAM 01 of a sample subjected to impact velocity of 197.8 m/s.

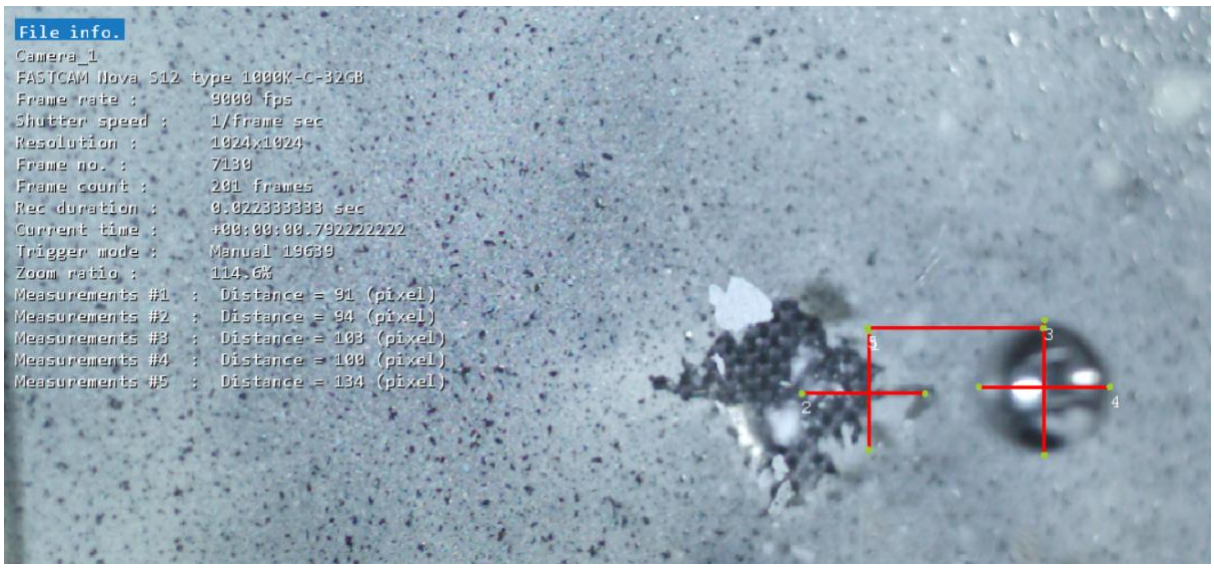

Figure 4.7: Calculation of apparent diameter and distances for CAM 01 of a sample subjected to 55.9 m/s impact velocity in PFV4

The residual velocities were thus calculated for each impact velocity as shown in Table 4.1

Table 4.1: Calculated residual velocities and corresponding impact velocities

Test Series	Impact Velocity (m/s)	Residual Velocity (m/s)	COV
IV-50	55.9	60.8 +/- 10.3	24.7
IV-80	80.0	83.23 +/- 16.5	2.8
IV-130	136.3	177.5 +/- 29.3	5.6
IV-190	197.8	191.7 +/- 27.1	-

As mentioned before, the scaling factor for the apparent diameter of the impactor was considered as it moves across the concerned time interval. Residual velocities were subsequently calculated based on both the initial and final instants of observation. It was observed that the calculated residual velocities exhibited considerable variation, encompassing a broad range of values. This variability can be attributed to the necessary approximations and the simplification of the trigonometric analysis adopted to facilitate processing and interpretation of the results.

Despite these approximations, it was found that the range of residual velocities for all tested specimens generally included the recorded impact velocity. Furthermore, although the minimum residual velocity values were, in most cases, lower than the initial impact velocities, the overall data suggests that there was minimal change in the velocity of the projectile post-impact. This finding is likely due to the thinness of the specimens, which limited significant energy transfer from the projectile during impact. As such, the chosen methodology did not detect a marked difference in projectile velocity, underscoring the influence of specimen thickness on energy dissipation in ballistic events.

4.1.3. Tomography analysis

X-ray computed tomography (CT) scans were performed on nine specimens using a high-resolution Nikon M2 450kV micro-CT system, capable of non-destructive 3D imaging. Detailed volumetric data of the facesheets and core was captured. Scan parameters were set to achieve optimal contrast between the damaged zone, porosities, skins, and foam core. The raw scan data was transferred and analysed using Hexagon's myVGL 2022/23 software. This enabled

the visualization of 2D slice images. The porosity analysis and measurement of delamination area were then carried out aligned with the x-z coordinate system.

Two-dimensional slice images were procured for each skin face, and 3 images were procured for the foam core. Moreover, porosity analysis was carried out for one slice each for the faces and one from the middle of the core. This also yielded the delamination area parallel to the face for each slice which corresponded to the x-z coordinate system on the software interface. Figure 4.8 shows the CT scan slices obtained from myVGL for a sample post-impact (136.3 m/s) corresponding to the faces and cores respectively.

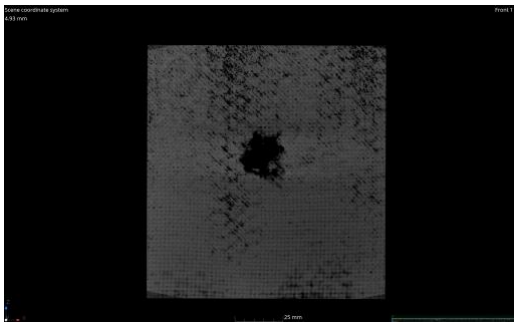

(a) impact side face skin

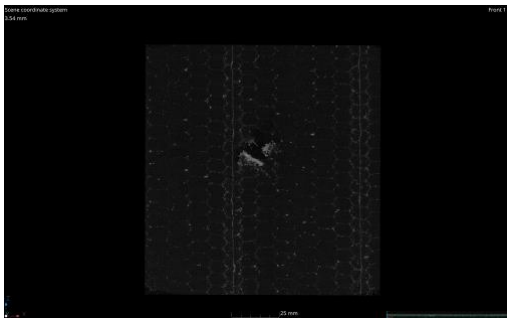

(b) core

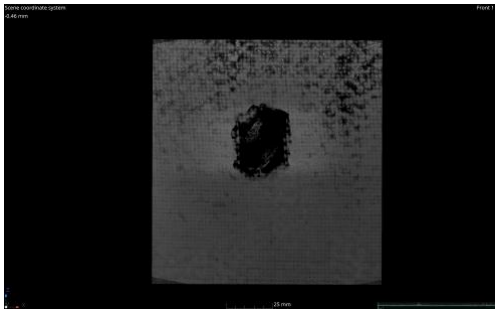

(c) non-impact side face skin

Figure 4.8: Tomographic scans of a post-impact panel subjected to 136.3 m/s

The CT scans correspond to the visual images of the exterior of the concerned panel. Moreover, the CT scan images of the core provide a clear visual representation of the damaged interior. Further porosity analysis of the core and the skins was carried out using myVGL. This yielded the area of damage numerically and visually. The area of damage for the

core was taken as the average of three 2D slices from the middle of the core at regular intervals.

Table 4.2 shows the average delamination area for face skins and foam core respectively corresponding to specimens under each impact and residual velocity. Figure 4.9 shows the general trend between the velocities and observed delamination areas for skins.

Table 4.2: Mean delamination area of face skins and core for each impact and residual velocity

Impact Velocity (m/s)	Residual Velocity (m/s)	Delamination area of skin (mm^2)		Damaged area of core (mm^2)	
		Mean	COV	Mean	COV
55.9	60.8 +/- 10.3	2463.8	0.535	1.3	0.040
80.0	83.23 +/- 16.5	1366.1	0.802	3.2	0.803
136.3	177.5 +/- 29.3	1662.2	0.277	0.9	0.707
197.8	191.7 +/- 27.1	819.7	0.179	3.5	-

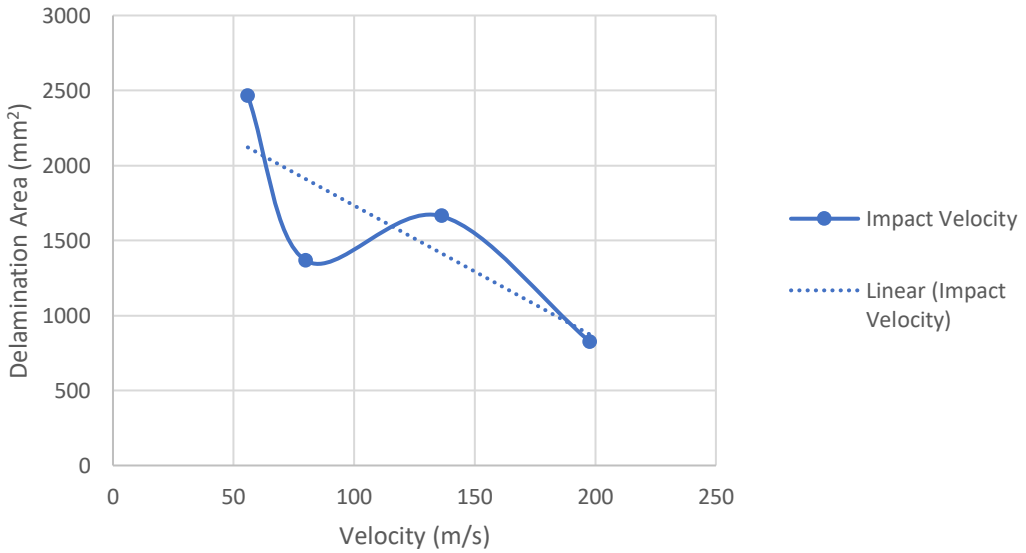

Figure 4.9: Plot of delamination area vs impact velocities for skin

In general, delamination area is smaller for the impact velocity at the higher end (197.8 m/s) and is larger for the lower impact velocity 55.9 m/s. The mid-tier impact velocities correspond to delamination areas falling in a similar medium range. Overall, a variance is observed among

the delamination areas across all samples. However, even among the variance, a general trend can be seen. This trend corresponds to a more focused and compact damaged area at higher velocities. The projectile passes straight through the specimen at higher velocities and does not have ample time to spread the area of damage. Also, a significant difference can be observed between the area of damage of skin and core in Table 4.2. The core has a much smaller delamination area. This can be a result of the foam's higher energy absorption capability.

4.2. Numerical Results

Finite element simulations were performed at the four impact velocities tested experimentally: 55.9, 80.0, 136.3, and 197.8 m/s. Field outputs for the Mises stress were requested at every 0.0003 s time increment for a smoother frame drop. The output requested was for the first layer of the impact-side facesheet to visualize the impact scenario. The visualization of the stress field pattern was then compared for all four impact velocities. For the velocities of 55.9, 80.0, and 136.3 m/s, a stress wave pattern emerged that dissipated radially outward simulating the experimental shock wave observed during high-impact scenarios as seen in Figure 4.10.

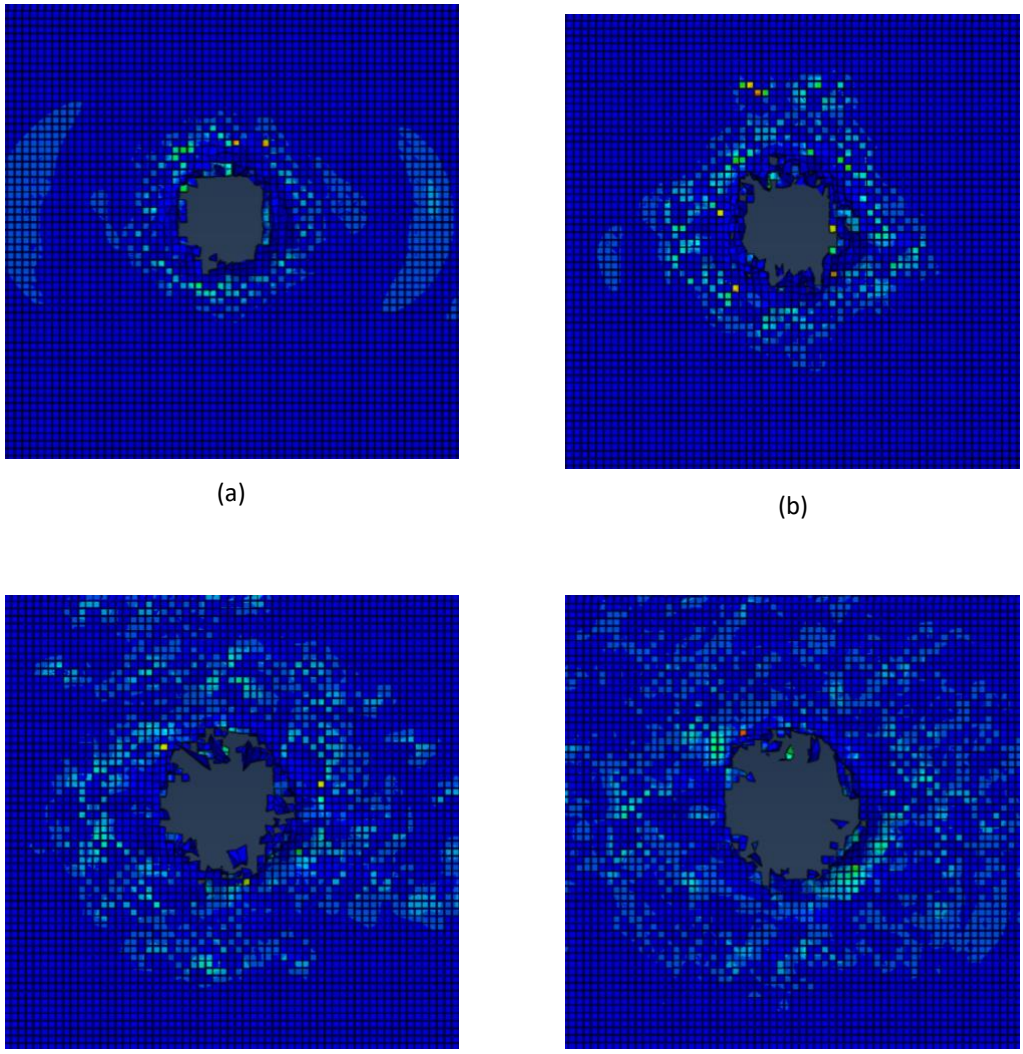

(a) (b)

(c) (d)

Figure 4.10: The stress field visualization for the panel impacted at 80.0 m/s at time increments (a) 0.6 ms (b) 0.9 ms (c) 1.5 ms (d) 2.1 ms from launch

Similarly, Figure 4.11 shows the projectile body as it moves through the specimen at 55.9 m/s at intervals of 0.6 ms from launch.

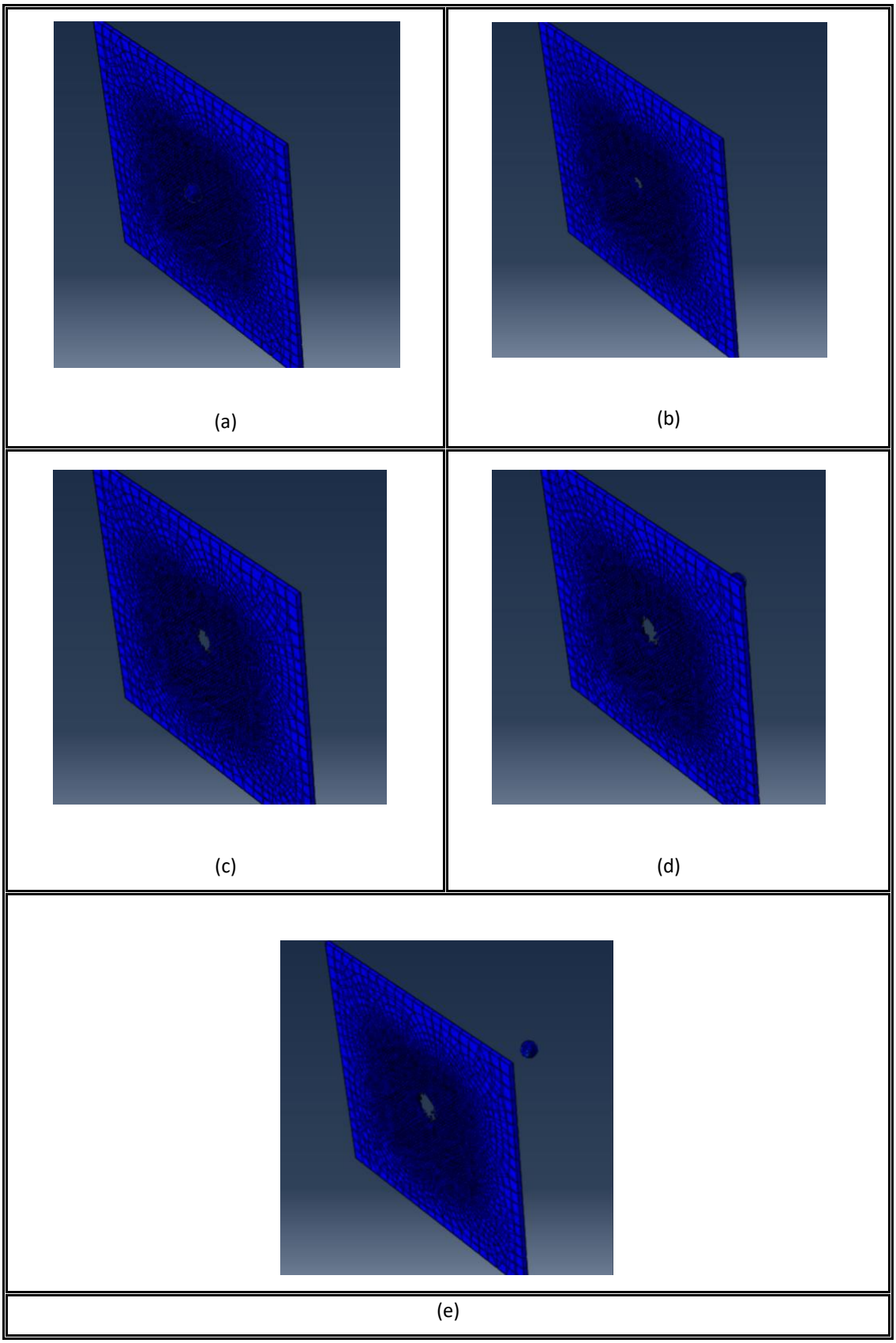

Figure 4.11: The movement of the projectile through the specimen at 55.9 m/s at time increments (a) 0.6 ms (b) 1.2 ms (c) 1.8 ms (d) 2.4 ms (e) 3.0 ms from launch

At the velocity of 197.8 m/s, the model showed numerical instability after the first two frames post-impact (0.6 ms) as seen in Figure 4.12. This can be attributed to the utilization of the Lagrangian approach of modelling that cannot simulate high strain rates accurately and results in structural distortion. This can be solved by the use of the Smoothed-Particle Hydrodynamics (SPH) modelling approach.

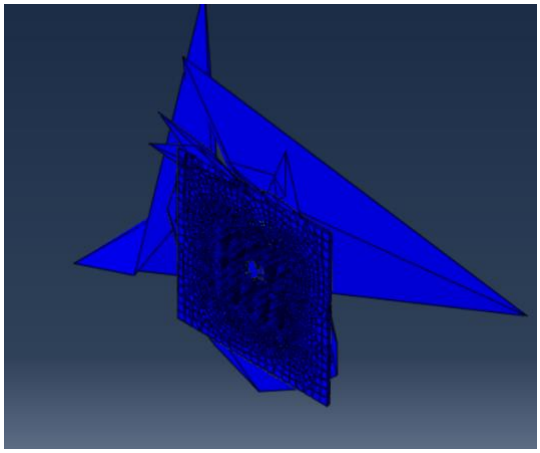

Figure 4.12: Observed numerical instability in the model at 197.8 m/s

The stresses observed at impact velocities of 55.6, 80, and 136.3 m/s are in the orders of 10^2 on average. Figure 4.13 shows a Mises stress output for the panel at an impact velocity of 80.0 m/s. Moreover, on average, the damaged area is approximately double that of the diameter of the projectile (19.05 mm).

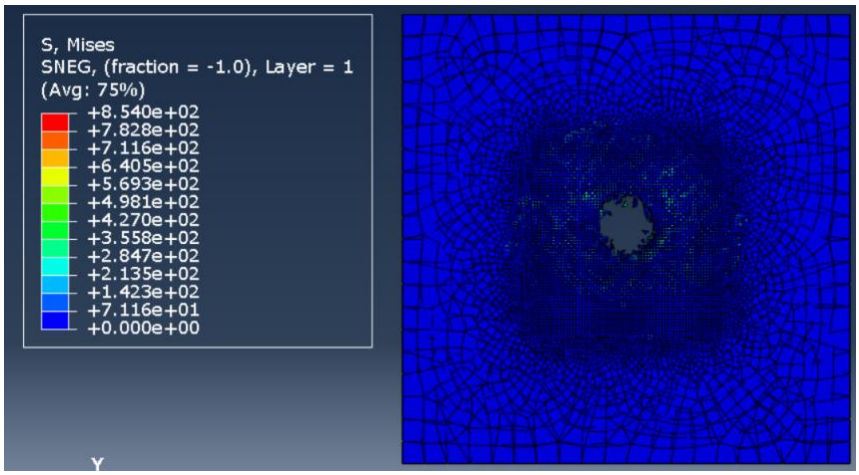

Figure 4.13: Mises stress field visualization for an impact velocity of 80.0 m/s

To accurately model the impact scenario, a more robust experimental dataset for the PET foam and an implementation of the VUMAT subroutine is required. Moreover, to validate the numerical results, stress and strain fields are needed through DIC. These areas remain unexplored in this study and can be addressed in future work.

THIS PAGE WAS INTENTIONALLY LEFT BLANK.

5. CONCLUSIONS

This chapter synthesises the findings of the experimental campaign and the numerical modelling conducted on CFRP–PET foam sandwich panels subjected to high-velocity impacts. It further outlines the limitations encountered during the study and highlights directions for future research.

5.1. Experimental Results

Nine CFRP-PET sandwich panels were tested at four different velocities to study the material response and behaviour. Complete perforation of the panels at the lowest impact velocities indicates limited energy absorption capabilities. The major contributing factor seems to be the low thickness of the facesheets and the panel as a whole. The experimentation highlighted that for such thin configurations, the sandwich panels provide minimal ballistic protection against impact velocities of at least 55.6 m/s. The ballistic limit is likely lower than the tested velocities.

The residual velocity analysis showed that the residual velocities remained close to the impact velocities. The vast range of the values obtained can be attributed to a simplistic approximation of a complex three-dimensional arrangement of the experimental setup. The cameras and projectile were assumed to lie in the same plane and vertical deflection was assumed to be negligible. Moreover, the scaling factor of the projectile as it travelled relative to camera position and manual measurement made it challenging to effectively procure accurate dimensions.

Tomographic scans further showed that damage was primarily concentrated in the face-sheets with the core exhibiting significantly smaller damaged areas. This indicated that the larger part of the energy absorption was carried out by the foam and the facesheets exhibited limited energy absorption capabilities.

Overall, these results reinforce that the low-thickness panels provide minimal ballistic protection, with damage highly localized and largely unaffected by increasing impact velocity. The concerned CFRP-PET foam sandwich panels do not perform comparably to their counterparts used commercially in aerospace applications under such high-impact scenarios. Enhancing the impact resistance and increasing the ballistic limit requires a redefinition of the dimensions (such as an increase in core thickness or skin layers), optimizing the architecture, or a reselection of materials.

5.2. Numerical Modelling

The finite element model developed in Abaqus/Explicit provided a first-order approximation of the panels' impact response, successfully reproducing stress wave propagation at moderate velocities (55.9–136.3 m/s). However, the model showed limitations in capturing the dynamic behaviour of the PET foam, as its constitutive response was simplified and strain-rate effects were not explicitly considered.

At the highest tested velocity (197.8 m/s), the model exhibited severe numerical instabilities. These instabilities stem from the inherent limitations of a purely Lagrangian approach, which becomes unreliable at very high strain rates due to mesh distortion. Without experimental validation—particularly through Digital Image Correlation (DIC)—the fidelity of the simulations remains unverified. The lack of accurate dynamic material data for the PET foam further restricted model reliability.

5.3. Future Work

This study opens several avenues for further investigation. Experimental efforts should prioritise the acquisition of reliable strain and stress fields through Digital Image Correlation, enabling both improved material calibration and robust validation of numerical models. Numerical work should consider advanced constitutive modelling strategies, including VUMAT/VUSDFLD subroutines for damage progression or alternative methods such as Smoothed-Particle Hydrodynamics (SPH) and Coupled Eulerian–Lagrangian (CEL) formulations to overcome Lagrangian instabilities at high velocities.

From a design perspective, future campaigns should investigate panels with increased core thickness, higher-density foams, and hybrid laminate architectures to improve energy dissipation and delay perforation. Parametric studies on projectile type (hard vs. soft body), geometry, and mass could further clarify failure mechanisms and inform optimisation strategies.

Taken together, these improvements could lead to sandwich structures with significantly enhanced impact resistance and energy absorption, bringing their performance closer to the stringent safety requirements of aerospace applications.

REFERENCES

[1] P. Seidenman, 'How Bird Strikes Impact Engines', *Aviation Week*, Oct. 07, 2016.

[2] J. R. Allan, 'THE COSTS OF BIRDSTRIKES TO COMMERCIAL AVIATION', 2001. [Online]. Available: https://digitalcommons.unl.edu/birdstrike2001

[3] M. Roberts, 'Is The Risk Of Drones Colliding With Commercial Aircraft Increasing?', *Simple Flying*, May 19, 2025.

[4] C. Ashe, '3rd CAB weathers hail storm', *U.S. Central Command*, Jun. 27, 2013.

[5] P. Qiao, M. Yang, and F. Bobaru, 'Impact Mechanics and High-Energy Absorbing Materials: Review', *J Aerosp Eng*, vol. 21, no. 4, pp. 235–248, Oct. 2008, doi: 10.1061/(asce)0893-1321(2008)21:4(235).

[6] A. Serge, *Impact on Composite Structures*. Cambridge University Press, 1998.

[7] H. Fang, E. Palta, and M. Gutowski, 'Numerical simulation of high-speed impacts involving metallic and non-metallic materials', *International Journal of Computational Methods and Experimental Measurements*, vol. 6, no. 3, pp. 463–475, 2018, doi: 10.2495/CMEM-V6-N3-463-475.

[8] J. D. Clayton, 'Analysis of adiabatic shear coupled to ductile fracture and melting in viscoplastic metals', Feb. 2025, [Online]. Available: http://arxiv.org/abs/2502.10625

[9] M. Kamran, H. Liu, D. Fukuda, P. Jia, G. Min, and A. Chan, 'State-of-the-Art Review and Prospect of Modelling the Dynamic Fracture of Rocks Under Impact Loads and Application in Blasting', *Geosciences (Basel)*, vol. 15, no. 8, p. 314, Aug. 2025, doi: 10.3390/geosciences15080314.

[10] I. Daniel and O. Ishai, *Engineering Mechanics of Composite Materials*. Oxford University Press, Inc., 1994.

[11] S. Chandra *et al.*, 'Experimental investigations on composite, fibre-metal and metal coupons for high velocity bird impacts', 2007.

[12] R. Vignjevic *et al.*, 'Soft body impact resistance of composite foam core sandwich panels with unidirectional corrugated and tubular reinforcements', *Int J Impact Eng*, vol. 132, Oct. 2019, doi: 10.1016/j.ijimpeng.2019.103320.

[13] D. Varas, J. López-Puente, and R. Zaera, 'Experimental and numerical study of high velocity impacts on carbon/epoxy laminates', EDP Sciences, 2009, pp. 1799–1805. doi: 10.1051/dymat/2009253.

[14] C. Rekatsinas *et al.*, 'Micromechanics-based multi-scale framework with strain-rate effects for the simulation of ballistic impact on composite laminates', *J Compos Mater*, vol. 58, no. 27, pp. 2897–2914, Nov. 2024, doi: 10.1177/00219983241283618.

[15] N. Toso and A. Johnson, 'LIBCOS-Significance of Load upon Impact Behaviour of Composite Structure Final report', 2011.

[16] S. Heimbs, 'Bird Strike Simulations on Composite Aircraft Structures', Munich, May 2011.

[17] K. S. Pandya, J. R. Pothnis, G. Ravikumar, and N. K. Naik, 'Ballistic impact behavior of hybrid composites', *Mater Des*, vol. 44, pp. 128–135, 2013, doi: 10.1016/j.matdes.2012.07.044.

[18] R. J. Muhi, F. Najim, and M. F. S. F. de Moura, 'The effect of hybridization on the GFRP behavior under high velocity impact', *Compos B Eng*, vol. 40, no. 8, pp. 798–803, Dec. 2009, doi: 10.1016/j.compositesb.2009.08.002.

[19] P. J. Hazell and G. Appleby-Thomas, 'A study on the energy dissipation of several different CFRP-based targets completely penetrated by a high velocity projectile', *Compos Struct*, vol. 91, no. 1, pp. 103–109, Nov. 2009, doi: 10.1016/j.compstruct.2009.04.036.

[20] E. P. Gellert, S. J. Cimpoeru, and R. L. Woodward, 'A study of the effect of target thickness on the ballistic perforation of glass-fibre-reinforced plastic composites', 2000.

[21] M. Guida, 'Study, Design and Testing of Structural Configurations for the Bird-Strike Compliance of Aeronautical Components', 2008.

[22] J. Tirillò *et al.*, 'High velocity impact behaviour of hybrid basalt-carbon/epoxy composites', *Compos Struct*, vol. 168, pp. 305–312, May 2017, doi: 10.1016/j.compstruct.2017.02.039.

[23] A. N. Yuksel Yilmaz, D. E. Yunus, and A. C. Bedeloglu, 'Investigation of mechanical properties of hybrid stainless steel/acrylic and carbon fiber reinforced epoxy composite', *J Compos Mater*, vol. 56, no. 18, pp. 2855–2866, Aug. 2022, doi: 10.1177/00219983221106249.

[24] M. A. Mccarthy, J. R. Xiao, N. Petrinic, A. Kamoulakos, and V. Melito, 'Modelling of Bird Strike on an Aircraft Wing Leading Edge Made from Fibre Metal Laminates-Part 1: Material Modelling', 2004.

[25] M. Wisnom *et al.*, 'TAKING ADVANTAGE OF THE HYBRID EFFECT IN THIN-PLY PSEUDO-DUCTILE LAMINATES', 2020. [Online]. Available: http://www.bristol.ac.uk/composites/

[26] J. Hu *et al.*, 'Pseudo-ductility behavior of carbon/glass hybrid composites with unidirectionally arrayed chopped strands: Experimental and numerical research', *Polym Compos*, vol. 45, no. 16, pp. 14741–14756, Nov. 2024, doi: 10.1002/pc.28796.

[27] S. A. Zachariah, S. Shenoy, and D. Pai, 'EXPERIMENTAL ANALYSIS OF THE EFFECT OF THE WOVEN ARAMID FABRIC ON THE STRAIN TO FAILURE BEHAVIOR OF PLAIN WEAVED CARBON/ARAMID HYBRID LAMINATES', *Facta Universitatis, Series: Mechanical Engineering*, vol. 22, no. 1, pp. 13–24, Apr. 2024, doi: 10.22190/FUME200819022Z.

[28] M. Y. Yuhazri *et al.*, 'The Effect of Lamina Intraply Hybrid Composites on the Tensile Properties of Various Weave Designs', in *IOP Conference Series: Materials Science and Engineering*, Institute of Physics Publishing, Dec. 2016. doi: 10.1088/1757-899X/160/1/012022.

[29] P. Kędzierski, A. Popławski, R. Gieleta, A. Morka, and G. Sławiński, 'Experimental and numerical investigation of fabric impact behavior', *Compos B Eng*, vol. 69, pp. 452–459, 2015, doi: 10.1016/j.compositesb.2014.10.028.

[30] M. Agrawal, R. T. Durai Prabhakaran, and P. Mahajan, 'Experimental investigations on the fatigue behavior of hybrid basalt/glass fiber epoxy composites', *Fatigue Fract Eng Mater Struct*, vol. 47, no. 7, pp. 2650–2667, Jul. 2024, doi: 10.1111/ffe.14303.

[31] I. Smojver and D. Ivančević, 'Bird strike damage analysis in aircraft structures using Abaqus/Explicit and coupled Eulerian Lagrangian approach', *Compos Sci Technol*, vol. 71, no. 4, pp. 489–498, Feb. 2011, doi: 10.1016/j.compscitech.2010.12.024.

[32] T. Wagner, S. Heimbs, F. Franke, U. Burger, and P. Middendorf, 'Experimental and numerical assessment of aerospace grade composites based on high-velocity impact experiments', *Compos Struct*, vol. 204, pp. 142–152, Nov. 2018, doi: 10.1016/j.compstruct.2018.07.019.

[33] E. Sevkat, B. Liaw, and F. Delale, 'Ballistic performance of hybrid and non-hybrid composite plates', *Journal of Strain Analysis for Engineering Design*, vol. 47, no. 7, pp. 453–470, Oct. 2012, doi: 10.1177/0309324712457897.

[34] S. R. Jammi, ‘BIRD STRIKE ANALYSIS OF A COMPOSITE AIRCRAFT WING’, 2015. [Online]. Available: http://www.asme.org/about-asme/terms-of-use

[35] A. Riccio, R. Cristiano, S. Saputo, and A. Sellitto, ‘Numerical methodologies for simulating bird-strike on composite wings’, *Compos Struct*, vol. 202, pp. 590–602, Oct. 2018, doi: 10.1016/j.compstruct.2018.03.018.

[36] L. Correia and F. Ribeiro, ‘Arnau Roca i Caellas Design and Evaluation of FRP Composite Engine Support Structures for Unmanned Aircraft Systems’, 2024.

[37] A. Gomez, S. Sanchez-Saez, and E. Barbero, ‘Influence of in-plane preload on the impact behavior of composite sandwich panels’, *Mechanics of Advanced Materials and Structures*, 2025, doi: 10.1080/15376494.2025.2489671.

[38] I. Ivañez, C. Santiuste, E. Barbero, and S. Sanchez-Saez, ‘Numerical modelling of foam-cored sandwich plates under high-velocity impact’, *Compos Struct*, vol. 93, no. 9, pp. 2392–2399, 2011, doi: 10.1016/j.compstruct.2011.03.028.